International Journal of Computational and Experimental Science and ENgineering (IJCESEN)

Vol. 11-No.1 (2025) pp. 1434-1443
http://www.ijcesen.com

ISSN: 2149-9144

Research Article

Evaluation of The Effect of Monochromatic Images Of Ti6Al4V Implant Material Obtained with Dual Energy CT on Radiotherapy Plans Using The Treatment Planning System and EGSnrc Monte Carlo Simulation

Elif Önal[1], Bahar Dirican[2]*, Türkay Toklu[3]

[1] Gülhane Education and Research Hospital, Radiation Oncology Department, 06010, Ankara-Turkiye
Email: elif_onal@hotmail.com - **ORCID:** 0000-0002-3909-3713

[2]Gülhane Education and Research Hospital, Radiation Oncology Department, 06010, Ankara-Turkiye
* **Corresponding Author Email:** diricanbahar@gmail.com-**ORCID:**0000-0002-1749-5375

[3]Yeditepe University, Department of Medical Physics,34750, Istanbul, Turkey
Email: toklu@yeditepe.edu.tr-**ORCID:** 0000-0002-5399-9394

Article Info:

DOI: 10.22399/ijcesen.918
Received : 02 January 2025
Accepted : 05 March 2025

Keywords :

Radiotherapy,
Dual Energy CT,
Ti6Al4V Implant,
Metal Artifact Reduction,
Monte Carlo Simulation.

Abstract:

This study aimed to evaluate the effect of Dual Energy Computed Tomography (DECT) imaging on radiotherapy planning for Ti6Al4V (grade 23), a high-density implant material, using the Treatment Planning System (TPS) and Monte Carlo (MC) simulation. For this purpose, Ti6Al4V implants with diameters of 6.4 mm and 28 mm were produced with a 3D printer and placed in a Cheese phantom. Single Energy Computed Tomography (SECT) and DECT images were obtained for each implant. SECT and DECT plans were created using TPS on SECT and DECT images. DECT plans were simulated using the BEAM nrc MC code system based on EGSnrc. For the reference plan consisting of the artefact-free image, the Cheese phantom SECT image consisting entirely of water equivalent material was transferred to the planning. In planning, implants were created virtually and reference plans were created. The obtained planning and simulation results were compared with the reference plan and dose errors in planning were determined. As a result of the study, it was observed that DECT imaging significantly increased the dose accuracy for the 6.4 mm diameter TI6Al4V implant compared to conventional planning. For the 28 mm diameter implant material, it was observed that DECT imaging decreased the success of artefact suppression, but significantly increased the dose accuracy in treatment planning. It was observed that DECT scanners could be used for simulation purposes in radiotherapy clinics for patients with Ti6Al4V implant material. The study needs to be extended to other high-density implant materials encountered in patients receiving radiotherapy.

1. Introduction

Computed tomography (CT) images are used to define the target volume and organs at risk (OAR) of the patient in radiotherapy (RT) treatment planning. The calculation of the treatment dose is based on the conversion of CT numbers (Hounsfield Units, HU) to electron densities (ρe)[1]. Radiation oncologists require detailed and accurate visualization of the anatomical structure for 3D reconstruction of both target volumes and organs at risk (OAR) of the patient to be treated. In patients with high-density implant material such as hip, shoulder, or dental implants, these implants may cause harmful artifacts in CT images. Metallic hardware causes severe beam hardening and significantly attenuates the X-ray degrading the image quality to the extent that the resulting image is either incomplete or an inaccurate projection of data causing in reconstruction artifacts [2]. However, metal artifacts adjacent to or even included in the target volume or nearby OARs impair dose calculations and render accurate target delineation difficult or even impossible [3].

DECT has been used in radiology departments in the world and in our country since 2006. DECT allows different materials in distinguishing the tissues to be distinguished by scanning the objects in two different energy spectra. Van Elmth al. (2016) conducted preliminary studies for radiotherapy and showed that the errors in dose estimation can be

reduced with better tissue segmentation and better tissue electron density estimation with DECT images compared to SECT images [4]. Bongers et al. (2015) valuated the effects of dual energy-based imaging and iterative metal artifact algorithm and their combination in hip prosthesis and dental implants [5]. In subjects with the hip prosthesis, Dual Energy Metal Artifact Reduction (DEMAR) and Iterative Metal Artifact Reduction (IMAR) resulted in a significant reduction in artifacts compared to standard reconstructions (33% vs. 56%, respectively. $p<0.05$ for DEMAR and IMAR), but the degree of artifact reduction was significantly higher for IMAR. In contrast, for dental implants, only IMAR showed a significant reduction in artifacts, while DEMAR did not (71% vs. 8% $p<0.01$ and $p=0.1$, respectively). Nevertheless, IMAR itself showed a significant reduction in dental artifacts, while DEMAR did not (71% vs. 8% $p<0.01$ and $p=0.1$, respectively). Bazalova et al. (2008) used DECT-based material extraction for tissue segmentation in Monte Carlo calculations [6]. As a result of this study for normal tissues, dose calculation errors were found to be less than 1% in all beam planes. Akyol et al. (2021) found a 12.3% dose increment in front of the implant when the scattered doses were calculated using the Pencil Beam (PB) algorithm with a Thermo Luminesans Dosimetry (TLD) dosimeter placed in the jaw region of the dry head of the Ti alloy dental implant [7]. This study was done with conventional CT using the extended HU scale. Beyzadeoglu et al. (2006) observed an 18% dose increment in the scattered dose value obtained with the PB algorithm just in front of the Ti implant for 6MV photon energy using TLD in the human mandible placed in the water [8]. Pawalowski et al (2020) have shown that the use of 70 keV pseudo monoenergetic image sets with IMAR provides a significant reduction of metal artifacts and low CT number errors around dense materials [9]. Therefore, Pawalowski et al (2020) determined DECT and IMAR to be an attractive alternative to high keV imaging with metallic implants especially, in the context of radiotherapy planning [9]. However, this study was limited to image evaluation and did not evaluate its contribution to radiotherapy treatment doses.

The current study was carried out for 4.43g/cm^3 Ti6Al4V (grade 23 alloy) used in the production of patient-specific implants at Gulhane Medical Design and Production Application and Research Centre, University of Health Sciences Turkey. For this purpose, implants produced in this centre of 6.4 mm and 28 mm diameter sizes were placed in the Cheese phantom. The produced materials were placed in the Cheese phantom to obtain SECT and DECT images were obtained and the results of the planning on these images were evaluated by treatment planning and Monte Carlo simulation.

2. Material and Metods

2.1. Implant material

Ti6Al4V alloys used in this study were produced using a 3D printer (Concept Laser M2 Cusing Metal 3D Printer, GE Addictive, Germany) at the University of Health Sciences, Gülhane Medical Design and Production Application and Research Centre. The Ti6Al4V alloy used in this study is a standard alloy with the trade name Ti6Al4V garade 23 Eli. The atomic composition of the alloy defined in the MC simulation with respect to molecular weight and physical density is shown in Table 1.

2.2. Acquisition of SECT and DECT images

The images required for the study were obtained using the extended HU scale with the GE brand Revolution model DECT device with a fast switching feature operating in the Radiology Department of Istanbul Yeditepe University Kosuyolu Hospital. SECT imaging at standard 120kVp was used for conventional planning. DECT images were used in dual-energy modes at 80kVp-120kVp energy values. From these images, monoenergetic image sets and their MAR algorithm image sets were created using DECT image processing methods.

A wooden plane was used during imaging to enable the computed tomography device couch in the radiology department to consistently function as the radiotherapy treatment couch. We have taken the same DECT and SECT imaging parameter protocols to be able to obtain comparable treatment plans. All the parameters except for the imaging energies were the same. The cheese phantom was placed on the CT device in a similar position for all the images with a 2.5 mm section thickness for Scanner Field of View (SFOV): large body and Display Field of View (DFOV): 35 cm. Imaging setups are given in Figure1.

2.3 Selection of DECT images for treatment planning

Ti6Al4V Eli (grade 23) implants with diameters of 6.4 mm and 28 mm were placed in Cheese phantom for two different sizes and DECT images were obtained. From these images, monoenergetic image sets at 70keV, 90keV, 110keV, 130keV, and 140keV and their MAR algorithm image sets were generated using DECT image methods. These images were evaluated by six radiation oncologists at the

Table 1. *Physical and chemical properties of the implant material*

Material	Chemical Composition	Physical Density (g/cm^3)	Relative Electron Density (g/cm^3)
Ti Alloy (Ti6Al4V Eli(Grade 23))	Ti,Al,V,Fe,C,O,N,H	4.43	3.92

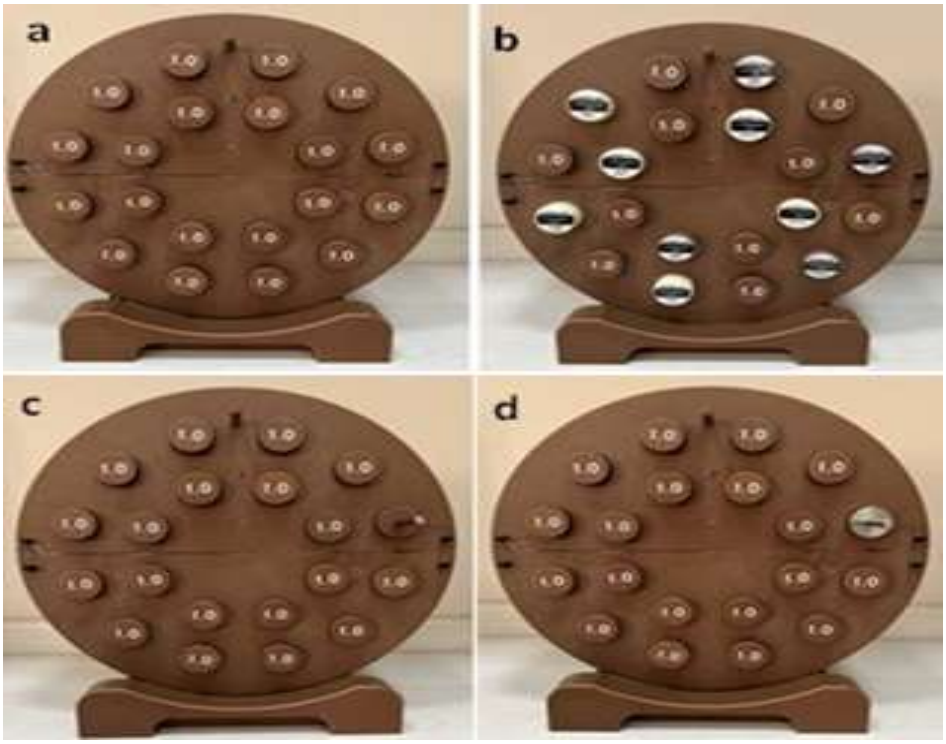

Figure 1. *Cheese Phantom Acquisition Images.* ***(A)*** *Phantom With Water Equivalent Plugs,* ***(B)*** *Phantom With Density Plugs,* ***(C)*** *Phantom With 6.4 mm Diameter Ti6Al4V Implants,* ***(D)*** *Phantom With 28 mm Diameter Ti6Al4V Implants.*

Radiation Oncology Clinic of Gülhane Training and Research Hospital, Health Sciences University Turkey. The SECT image obtained with 120kVp was accepted as an evaluation criteria reference and the image sets obtained from DECT images were compared with this image. In the comparison of the images, the image with the sharpest and least scattering of the implant material was considered the best, and the image with the least sharpness and the most scattering was considered the worst. The best 3 images according to the reference image were also ranked by the physicians.

The ranking order was done separately for the 6.4 mm Ti6Al4V and 28 mm TiAl4V implants and the images evaluated by the radiation oncologists are shown in Figure 2 for the 6.4 mm Ti6Al4V implant and Figure 3 for the 28 mm TiAl4V implant. The results of the ranking order are shown in Table 2 for the 6.4 mm Ti6Al4V implant and Table 3 for the 28 mm TiAl4V implant.

The DECT image planning sets chosen for each implant based on the evaluations of radiation oncologists are shown in Table 4.

2.4. Treatment planning

In this study, treatment planning was done using the Monaco (v.5.10.04, Elekta) treatment planning system and MC algorithm for the Elekta brand Synergy model linear accelerator device available in the Radiation Oncology Clinic of Health Sciences University. Treatment planning was done for the head first position. The implanted surface of the Cheese phantom was considered as the head in planning. Therefore, the image of the Cheese phantom in the planning is the exact reflection of the image seen in the CT scan. For treatment planning, the center of the homogeneous region of the 6.4 mm and 28 mm diameter implants placed in the Cheese phantom was determined as the center of the treatment area. All treatment plans were made for the 6 MV photon beam. The plans were calculated for 200 MU by the Monte Carlo algorithm with an area size of 20 cm x 4 cm, Gantri 270^{o} , Collimation 0^{o} , and the center of the phantom at the midline of the area where the implants were placed on the Cheese phantom as isocenter.

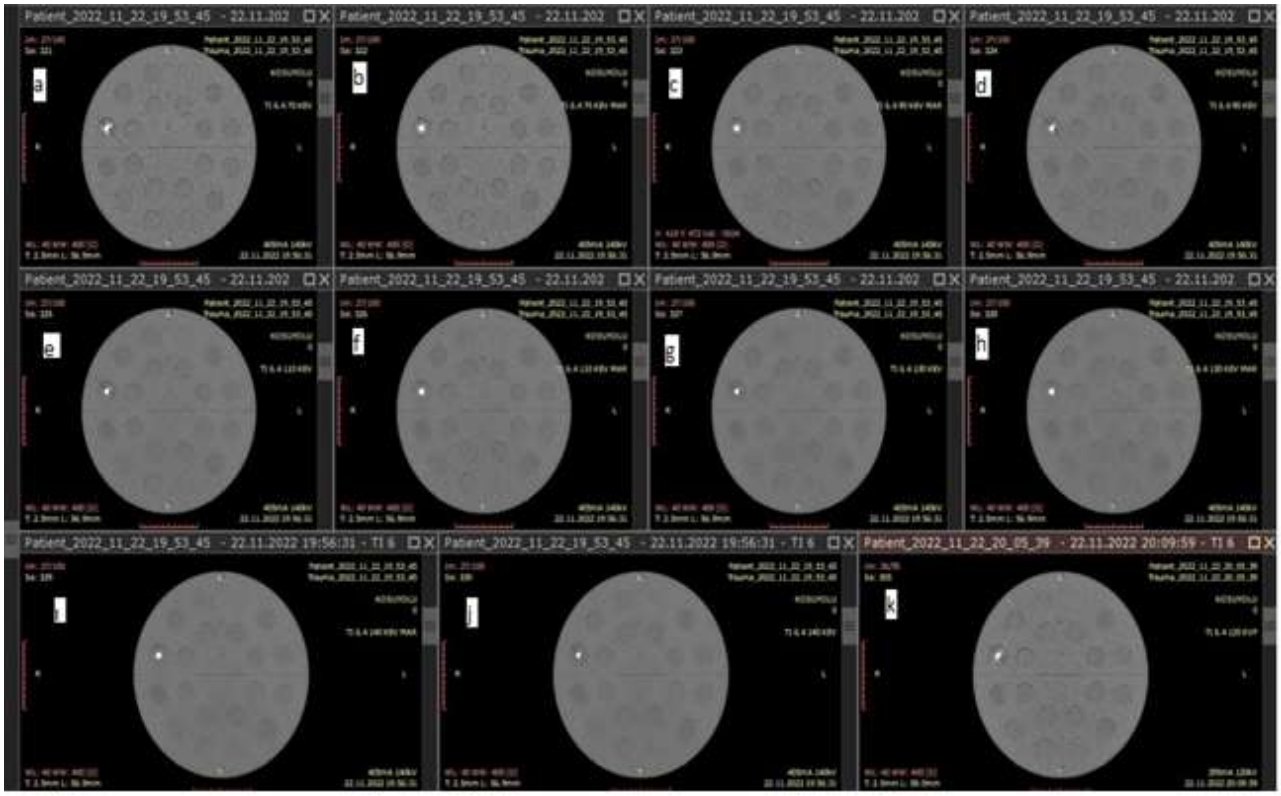

Figure 2. *Dual energy image sets obtained for 6.4mm Ti6Al4V implant**: (a)**70keV monoenergetic (mono) image, (b)70keV mono+MAR (monoenergetic+metal artefact reduction) image, **(c)**90keV mono+MAR image, **(d)**90keV mono image, **(e)**110keV mono image, (f)110keV mono+MAR image, **(g)**130keV mono+MAR image, **(h)**130keV mono image, **(i)**140keV mono image , **(j)**140keV mono+MAR image, **(k)**120kVp Single energy reference image*

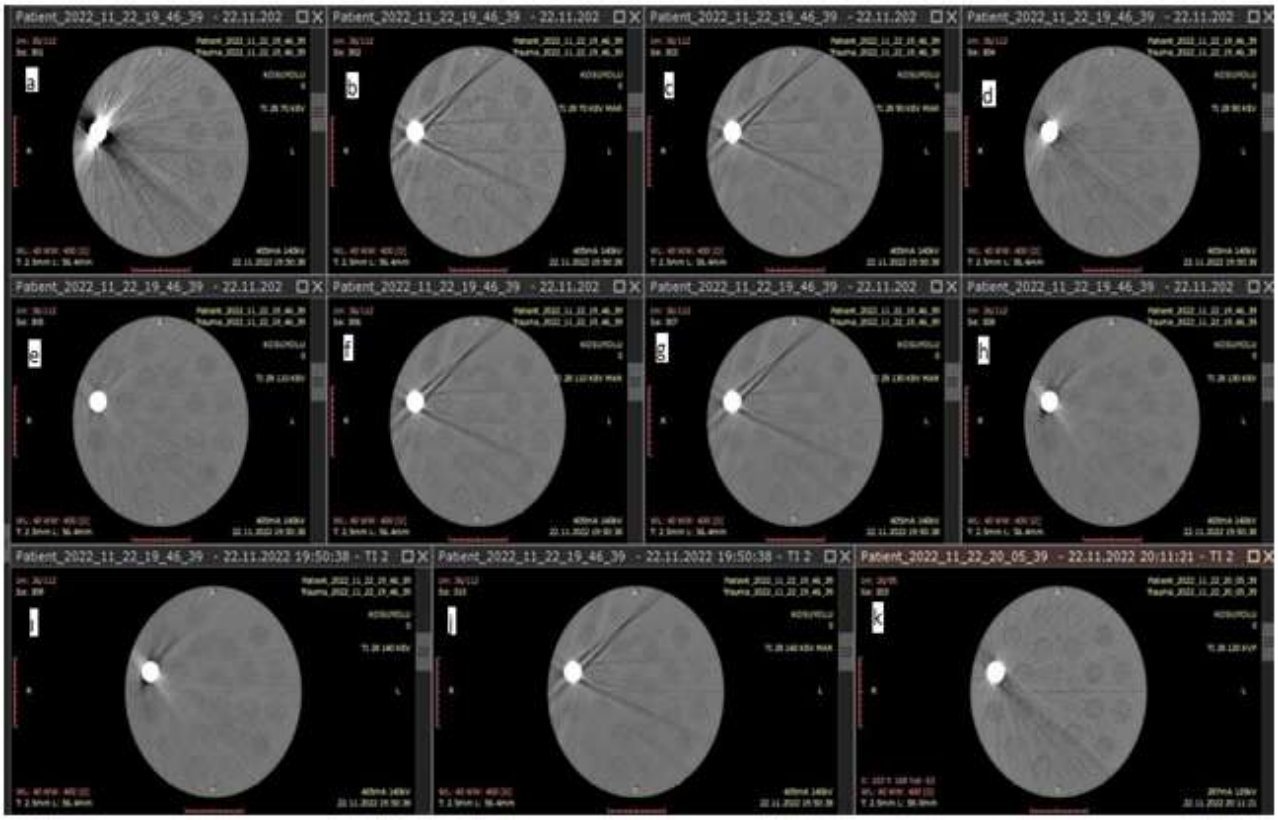

Figure 3. *Dual energy image sets obtained for 28mm Ti6Al4V implant**: (a)**70keV monoenergetic (mono) image, (b)70keV mono+MAR (monoenergetic+metal artefact reduction) image, **(c)**90keV mono+MAR image , **(d)**90keV mono image, **(e)**110keV mono image, (f)110keV mono+MAR image, **(g)**130keV mono+MAR image, **(h)**130keV mono image, **(i)**140keV mono image , **(j)**140keV mono+MAR image, **(k)**120kVp Single energy reference image*

Table 2. *Ranking order of DECT image sets of radiation oncologists for 6.4mm Ti6Al4V implant*

Ti6Al4V 6.4 mm	**Best image order**		
Radiation Oncologist	**1.**	**2.**	**3.**
1	110 keV mono+ MAR	130 keV mono+ MAR	140 keV mono+ MAR
2	140 keV mono+ MAR	130 keV mono+ MAR	110 keV mono+ MAR
3	140 keV mono+ MAR	130 keV mono+ MAR	110 keV mono+ MAR
4	140 keV mono+ MAR	130 keV mono+ MAR	110 keV mono+ MAR
5	90 Kev mono+ MAR	130 keV mono+ MAR	140 keV mono+ MAR
6	140 keV mono+ MAR	130 keV mono+ MAR	110 keV mono+ MAR

Table 3. *Ranking order of DECT image sets of radiation oncologists for 28 mm Ti6Al4V implant*

Ti6Al4V 28 mm	**Best image order**		
Radiation Oncologist	**1.**	**2.**	**3.**
1	110 keV mono	140 keV mono	130 keV mono
2	110 keV mono	140 keV mono	130 keV mono
3	110 keV mono	130 keV mono	140 keV mono
4	110 keV mono	130 keV mono	140 keV mono
5	110 keV mono	130 keV mono	140 keV mono
6	110 keV mono	130 keV mono	140 keV mono

Table 4. *DECT image planning sets chosen by radiation oncologists*

Implant	**Selected DECT Image Set**
6.4 mm Ti6Al4V implant	140 keV mono+ MAR
28 mm Ti6Al4V implant	110 keV mono

2.5. Monte Carlo Simulation

The 6-MV photon beam of the Elekta Synergy Linac was simulated with the EGSnrc-based MC code system BEAMnrc (Version, 2010) [10,11]. The component modules (CMs) SLABS, CONS3R, SLABS, FLATFILT, CHAMBER, MIRROR, JAW, MLCE, and MLCQ of BEAMnrc were used to simulate the target, primary collimator, vacuum window, flattening filter, ion chamber, mirror, jaws, and multileaf collimators, respectively. The total electron and photon cut-off energies - ECUT and PCUT were 0.7 and 0.01 MeV, respectively. Variance reduction techniques such as Directional Bremsstrahlung Splitting (DBS) were used to improve computational efficiency [12].To determine the optimum average energy of the initial electron beam, simulations with an average energy between 5.4 and 6.6 MeV in 0.2 MeV increments and a 1 MeV FWHM energy distribution were used. Using a 10×10 cm^2 open field and 1×10^9 initial particles, simulations were done with a $30 \times 30 \times 30$ cm^3 water phantom with a Source-Skin Distance (SSD) of 100 cm. The water phantom had $2 \times 2 \times 2$ mm^3 voxels. Three-dimensional dose distributions, percentage depth dose (PDD), and profile curves were obtained for each initial electron beam energy. The minimum difference between MC and ion chamber measurements was obtained at an average energy of 6.0 MeV. After the optimization run, the percentage depth dose (PDD) differences up to 30 cm depth of water were less than 1% for a 10×10 cm^2 open field. Since one monitor unit (MU) of the linac results in 1 cGy dose absorption in the water phantom at the maximum dose depth (dmax) (which is 1.5 cm for 6 MV photon beams), a similar calibration was applied for the MC simulation. A single dose pixel of $3 \times 3 \times 3$ mm^3 was placed in a $30 \times 30 \times 30$ cm^3 water phantom at a depth of 1.5 cm on the central axis of the photon beam for calibration. Using a 10×10 cm^2 open field and 2×10^9 initial particles, the dose to the dose pixel was calculated in units of dose per particle. From this calibration, it was determined that 1.1236×10^{15} particles were required to absorb 1 cGy at dmax. In this study, to compare the MC dose distribution with the dose distribution obtained from the TPS, the CT number - Relative electron density conversion defined in the TPS was used for the CT number - Physical density conversion in the MC simulation. For the conversion of relative electron density to physical density, the bi-linear transformation obtained from the use of Cheese Fantom electron density implants was used. The results are shown in Figure 4.

2.6. Evaluation and Analysis of Data

In this study, plans obtained from SECT and DECT images were analyzed in the presence of artifact-

forming implant materials. For ideal planning without artifacts, the Cheese phantom was filled with water-equivalent material, and 120 kVp single energy computed tomography images were loaded into the treatment planning system. While planning on these images, each implant was virtually contoured in the Monaco treatment planning system and the relative electron density values of the created structures were manually defined in the treatment planning system. In this way, treatment plans were created for the ideal situation and these plans were accepted as the reference treatment plan (TPref) in our data analyses. Treatment plans obtained from SECT images are defined as (TP_{SE}) and treatment plans obtained from DECT images are defined as (TP_{DE}) in TPS.

TPDE plans were simulated with the EGSnrc MC simulation program and simulation dose values were evaluated as TP_{SIM} results.

The relative dose differences between the dose values obtained from the reference treatment plan and TP_{SE}, TP_{DE}, and TP_{SIM} were calculated by the following formulas;

The difference (%) of TP_{SE} dose distribution from TP_{ref} dose distribution is as shown in Eq.(1);

$$Difference(\%) = \frac{D_{ref} - D_{SE}}{D_{ref}} \times 100 \quad (1)$$

The difference (%) of TP_{DE} dose distribution from TP_{ref} dose distribution is as shown in Eq.(2);

$$Difference(\%) = \frac{D_{ref} - D_{DE}}{D_{ref}} \times 100 \quad (2)$$

The difference (%) of TP_{SIM} dose distribution from TP_{ref} dose distribution is as shown in Eq.(3);

$$Difference(\%) = \frac{D_{ref} - D_{SIM}}{D_{ref}} \times 100 \quad (3)$$

3. Results and Discussions

Treatment plans were done for each implant material in SECT and DECT images, and the results were obtained by simulating the DECT plan in the EGSnrc program. The dose distributions obtained from the planning were transferred to PTW Verisoft software (Version 7.0, PTW-Freiburg). The dose distributions in the transverse section of the isocenter in the Cheese phantom were compared for two separate lines along the beam, the isocenter line and the implant center. Comparison results for 6.4 mm Ti6Al4V are shown in Figure 5 and for 28 mm Ti6Al4V in Figure 6. For 6.4 mm Ti6Al4V and 28 mm Ti6Al4V implant materials, the relative differences of the dose values in the transverse axis in the isocenter from the reference plan and the horizontal axis passing through the implant center in the phantom are shown in Table 5, and horizontal central axis in the phantom in Table 6.

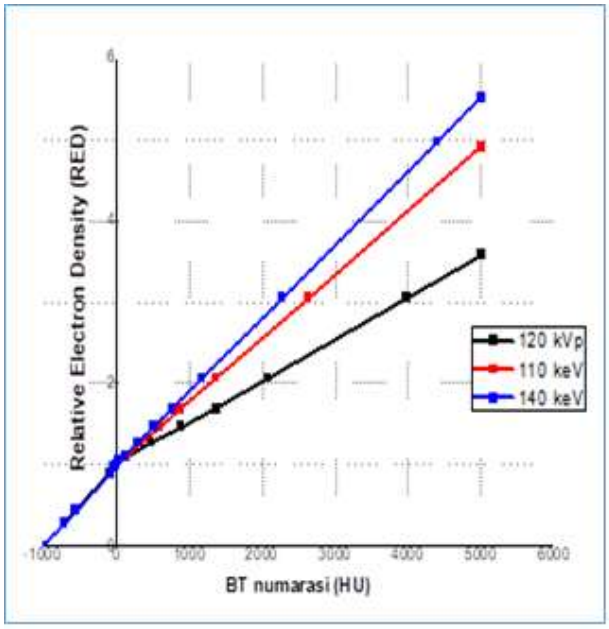

Figure 4. *HU-RED curves for the energies used in planning*

In this study, artifact reduction with DECT or DECT-MAR imaging for two different sizes of Ti6Al4V implant material, 6.4 mm and 28 mm in diameter, and their effect on radiotherapy treatment planning were examined. The planning results obtained from virtually generated reference plans, SECT and DECT images of the implants, and MC simulation results of the DECT plan were examined for comparison.

Two major methods have been defined in the literature for the reduction of metal artefacts. These are dual-energy computed tomography (DECT) virtual monochromatic extrapolations [3] and metal artifact reduction (MAR) algorithms [13,14]. Besides radiation is well studied in recent works [15-23], Wang at al.(2013) and Yu at al. (2012) have reported that DECT virtual monochromatic images between 95 and 150 keV levels effectively reduce beam hardening artifacts from various metallic prostheses [24,25]. In this study, the best image set for Ti6Al4V implant material determined by the physicians was 140keV monochromatic with MAR for a 6.4mm implant diameter and 110keV monochromatic image set for a 28mm implant diameter. These images were obtained from shots taken in the extended HU range. As yet there is no study using extended HU curves of SECT and DECT images for Ti6Al4V implant material and EGSnrc MC simulation obtained from DECT images evaluated together.

Akyol et al (2021) observed a dose increment in front of the Ti alloy implant and a dose decrease behind it [7]. In this study, similar results were obtained by evaluating the planning results obtained from DECT images. The results of the current study

are summarized in Table 5 and Table 6. The reason why the dose change at the entrance and exit of this implant could not be detected in SECT planning is the maximum distinguishable RED value for 120kVp images in the Elekta Monaco planning system is 3.58, whilst the actual RED of TI6Al4V is 3.92. Since the planning system does not detect the real RED value, it cannot calculate the real dose values in front of and behind the implant. Since the maximum RED values used in the planning obtained from DECT images were above the RED value of the Ti6Al4V implant material, the implant material was correctly included in the calculation of DECT planning. The reason for the lower simulated dose results around the implant compared to the reference plan is the phenomenon of partial volume effect [26]. High physical density changes within a voxel are uniformly represented in CT images. Thus, the HUs in the boundary voxels are the average of the HUs of the implant material and soft tissue, whereas all backscattered electrons are generated in the boundary voxels, resulting in small dose increases just in front of the implant material.

In this study, the effect of SECT and DECT imaging of Ti6AL4V implant materials with 6.4mm and 28mm diameters on the radiotherapy plan was examined. For 6.4mm diameter Ti6Al4V implant material, the relative dose difference of the planning results obtained from the SECT image from the reference plan was determined in the range of 0.45%-10.95% in the treatment field. The relative dose difference of the planning results obtained from DECT images from the reference plan was 0.11%-7.63%, and the relative dose difference of the results obtained from MC simulation from the reference plan was 0.45%-4.74%. Here, the maximum error obtained from the SECT image is in the high dose region just behind the implant line, while for the DE plan in DECT imaging, this maximum error is in the exit region where the treatment dose drops. Although the dose differences in this low-dose region are large in percentage terms, they represent dose differences of a few cGy. For 28mm Ti6Al4V implant material, the relative dose differences of the dose results obtained from SECT images, dose results obtained from DECT planning, and MC simulation results obtained from DECT imaging from the reference plan were determined to be (1.95%-20.58%); (0.41%-7.98%); and (1.28%-5.54%), respectively.

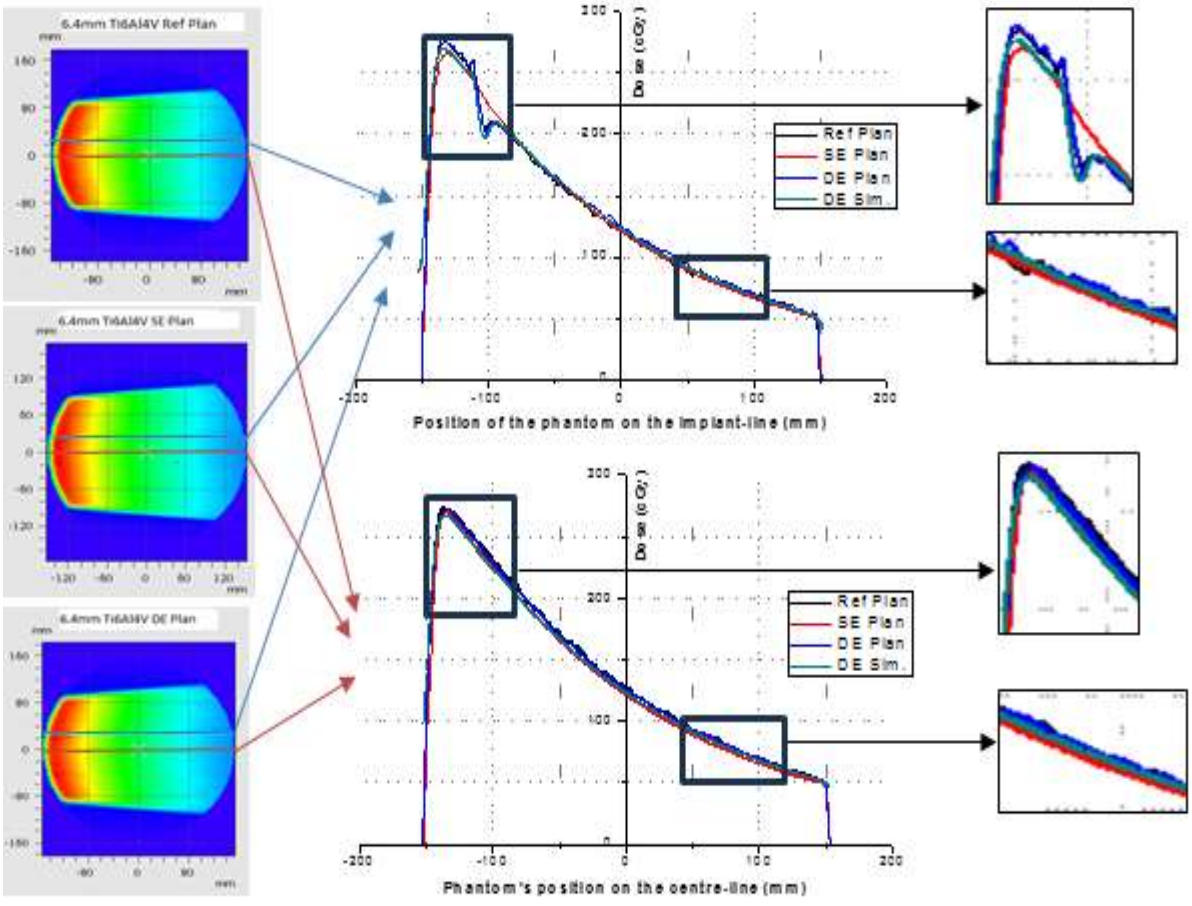

Figure 5. *Treatment plans and simulation results for the 6.4 mm Ti6Al4V implant for the implant centre-line and bundle centre-line along the bundle orientation in the transverse section at the plan isocenter.*

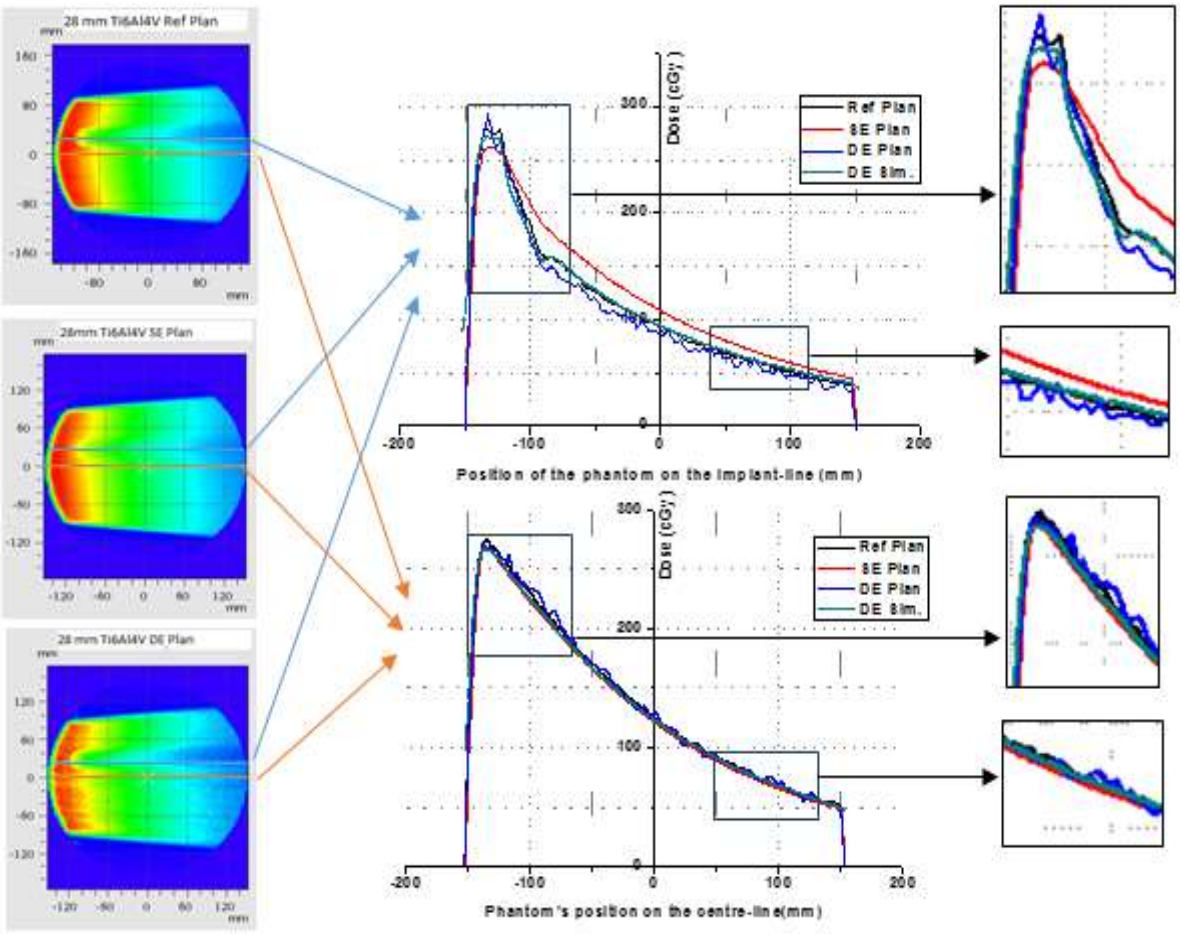

Figure 6. *Treatment Plans And Simulation Results For The 28 mm Ti6Al4V Implant For The Implant Centre-Line And Bundle Centre-Line Along The Bundle Orientation In The Transverse Section At The Plan Isocenter*

Table 5. *Relative dose differences of the dose values in the transverse axis at the isocenter from the reference plan for 6.4 mm Ti6Al4V and 28 mm Ti6Al4V implant materials are given for the horizontal axis passing through the line at the implant centre.*

Implant Material	Plan	Front of the implant	Behind the Implant	At -50mm from the centre	At the centre	At 50mm from the centre	At 100mm from the centre
6.4mm Ti6Al4V	SE Plan	-3,31	10,95	1,42	-1,55	1,25	-0,45
	DE Plan	0,64	-2,79	2,35	2,20	7,63	4,65
	Simulation	-4,67	-4,74	1,98	0,45	4,6	2,85
28mm Ti6Al4V	SE Plan	-6,54	17,77	16,51	20,58	16,21	17,43
	DE Plan	-2,87	-7,98	-5,69	-3,89	-7,38	-5,74
	Simulation	-3,75	-3,87	4,67	4,67	1,88	5,54

Table 6. *The differences of the dose values in the transverse axis at the isocenter from the reference plan for 6.4mm Ti6Al4V and 28mm Ti6Al4V implant materials are given for the horizontal axis passing through the line at the centre of the phantom.*

Implant Material	Plan	At -100mm from the centre	At -50mm from the centre	At the centre	At 50mm from the centre	At 100mm from the centre
6.4mm Ti6Al4V	SE Plan	-2,76	-3,61	-4,26	-4,71	-6,95
	DE Plan	-1,08	0,35	-1,18	-0,11	-0,14
	Simulation	-3,47	-2,62	-2,76	3,40	-3,40
28mm Ti6Al4V	SE Plan	-3,08	-2,87	-2,73	-3,78	-1,95
	DE Plan	-1,74	-0,41	4,25	-1,30	4,79
	Simulation	-2,30	-2,34	-1,28	-1,40	1,50

4. Conclusions

Ti6Al4V implant material was assessed to be more successful in artifact reduction with DECT imaging than conventional SECT imaging. However, an increase in the diameter of the implant material reduced this artifact suppression success. It can be concluded that the monochromatic images obtained with DECT imaging and the accompanying MAR algorithm reduce errors in radiotherapy planning. Nevertheless, in patients with Ti6Al4V implant material, DECT imaging provides us with the opportunity to create image sets at different monoenergetic levels and MAR versions of these image sets. These procedures do not require an additional dose to the patient and help to reduce the artefacts in the image. It prevents unnecessary dose exposure in patients and is a promising method for radiotherapy treatment planning.

Author Statements:

- **Ethical approval:** The conducted research is not related to either human or animal use.
- **Conflict of interest:** The authors declare that they have no known competing financial interests or personal relationships that could have appeared to influence the work reported in this paper
- **Acknowledgement:** This work was partially supported by The Scientific and Technological Research Council of Turkey (TÜBİTAK) grant (221S086).
- **Author contributions:** The authors declare that they have equal right on this paper.
- **Funding information:** This work was partially supported by The Scientific and Technological Research Council of Turkey (TÜBİTAK) grant (221S086).
- **Data availability statement:** The data that support the findings of this study are available on request from the corresponding author. The data are not publicly available due to privacy or ethical restrictions.

References

[1] Schwahofer A, Bär E, Kuchenbecker S, Grossmann JG, Kachelrieß M, Sterzing F. (2015) The application of metal artifact reduction (MAR) in CT scans for radiation oncology by monoenergetic extrapolation with a DECT scanner. *Zeitschrift fur medizinische Physik*. 25(4):314-325. doi:10.1016/j.zemedi.2015.05.004

[2] Stradiotti P, Curti A, Castellazzi G, Zerbi A. (2009) Metal-related artifacts in instrumented spine. Techniques for reducing artifacts in CT and MRI: state of the art. *European spine journal : official publication of the European Spine Society, the European Spinal Deformity Society, and the European Section of the Cervical Spine Research Society*. 18 Suppl 1(Suppl 1):102-8. doi:10.1007/s00586-009-0998-5

[3] Bamberg F, Dierks A, Nikolaou K, Reiser MF, Becker CR, Johnson TR. (2011) Metal artifact reduction by dual energy computed tomography using monoenergetic extrapolation. *European radiology*. 21(7):1424-9. doi:10.1007/s00330-011-2062-1

[4] Van Elmpt W, Landry G, Das M, Verhaegen F. (2016) Dual energy CT in radiotherapy: Current applications and future outlook. *Radiother Oncol*. 119(1):137-144. doi:10.1016/j.radonc.2016.02.026

[5] Bongers MN, Schabel C, Thomas C, et al. (2015) Comparison and Combination of Dual-Energy- and Iterative-Based Metal Artefact Reduction on Hip Prosthesis and Dental Implants. *PloS one*. 10(11);e0143584. doi:10.1371/journal.pone.0143584

[6] Bazalova M, Carrier JF, Beaulieu L, Verhaegen F. (2008) Dual-energy CT-based material extraction for tissue segmentation in Monte Carlo dose calculations. *Physics in medicine and biology*. 53(9);2439-56. doi:10.1088/0031-9155/53/9/015

[7] Akyol O, Olgar T, Toklu T, Eren H, Dirican B. (2021). Dose distrubution evaluation of different dental implants on a real human dry-skull model for head and neck cancer radiotherapy. *Radiation Physics and Chemistry*.189;109751.

[8] Beyzadeoglu M, Dirican B, Oysul K, Ozen J, Ucok O. (2006) Evaluation of scatter dose of dental titanium implants exposed to photon beams of different energies and irradiation angles in head and neck radiotherapy. *Dento maxillo facial radiology*. Jan 35(1):14-7. doi:10.1259/dmfr/28125805

[9] Pawałowski B, Panek R, Szweda H, Piotrowski T. (2020). Combination of dual-energy computed tomography and iterative metal artefact reduction to increase general quality of imaging for radiotherapy patients with high dense materials. Phantom study. *Physica medica : PM : an international journal devoted to the applications of physics to medicine and biology : official journal of the Italian Association of Biomedical Physics (AIFB)*. Sep 2020;77:92-99. doi:10.1016/j.ejmp.2020.08.009

[10] Kawrakow I. (2000). Accurate condensed history Monte Carlo simulation of electron transport. I. EGSnrc, the new EGS4 version. *Medical physics*. 27(3);485-98. doi:10.1118/1.598917

[11] Rogers DW, Faddegon BA, Ding GX, Ma CM, We J, Mackie TR. (1995). BEAM: a Monte Carlo code to simulate radiotherapy treatment units. *Medical physics*. 22(5);503-24. doi:10.1118/1.597552

[12] Kawrakow I, Rogers DW, Walters BR. (2004). Large efficiency improvements in BEAMnrc using directional bremsstrahlung splitting. *Medical physics*. 31(10):2883-98. doi:10.1118/1.1788912

[13] Meyer E, Raupach R, Lell M, Schmidt B, Kachelriess M. (2010). Normalized metal artifact reduction (NMAR) in computed tomography. *Medical physics*. 37(10):5482-93. doi:10.1118/1.3484090

[14] Lell MM, Meyer E, Schmid M, et al. (2013). Frequency split metal artefact reduction in pelvic computed tomography. *European radiology*. Aug 23(8);2137-45. doi:10.1007/s00330-013-2809-y

[15]Abuş, F., Gürçalar , A., Günay, O., Tunçman , D., Kesmezacar, F. F., & Demir, M. (2024). Determination of Radiation Dose Levels Incurred by Lenses During Scopy Imaging. *International Journal of Applied Sciences and Radiation Research* , 1(1). https://doi.org/10.22399/ijasrar.11

[16]gul, osman vefa, Demir, hikmettin, Kanyilmaz, G., & Cakır, T. (2024). Dosimetric comparison of 3D-Conformal and IMRT techniques used in radiotherapy of gastric cancer: A retrospective study. *International Journal of Computational and Experimental Science and Engineering,* 10(1). https://doi.org/10.22399/ijcesen.296

[17]Serap ÇATLI DİNÇ, AKMANSU, M., BORA, H., ÜÇGÜL, A., ÇETİN, B. E., ERPOLAT, P., … ŞENTÜRK, E. (2024). Evaluation of a Clinical Acceptability of Deep Learning-Based Autocontouring: An Example of The Use of Artificial Intelligence in Prostate Radiotherapy. *International Journal of Computational and Experimental Science and Engineering,* 10(4). https://doi.org/10.22399/ijcesen.386

[18]Özlen, M. S., Cuma, A. B., Yazıcı, S. D., Yeğin, N., Demir, Özge, Aksoy, H., … Günay, O. (2024). Determination of Radiation Dose Level Exposed to Thyroid in C-Arm Scopy. *International Journal of Applied Sciences and Radiation Research* , 1(1). https://doi.org/10.22399/ijasrar.13

[19]MOHAMMED, H. A., Adem, Şevki, & SAHAB, K. S. (2023). Optimal Examination Ways to follow up patients effected by COVID-19: case study in Jalawla General Hospital in Iraq. *International Journal of Applied Sciences and Radiation Research* , 1(1). https://doi.org/10.22399/ijasrar.5

[20]Çağlan, A., & Dirican, B. (2024). Evaluation of Dosimetric and Radiobiological Parameters for Different TPS Dose Calculation Algorithms and Plans for Lung Cancer Radiotherapy . *International Journal of Computational and Experimental Science and Engineering,* 10(2). https://doi.org/10.22399/ijcesen.335

[21]Vural, M., Kabaca, A., Aksoy, S. H., Demir, M., Karaçam, S. Çavdar, Ulusoy, İdil, … Günay, O. (2025). Determination Of Radiation Dose Levels to Which Partois And Spinal Cord (C1-C2) Regions Are Exposed In Computed Tomography Brain Imaging. *International Journal of Applied Sciences and Radiation Research* , 2(1). https://doi.org/10.22399/ijasrar.17

[22]Waheed, F., Mohamed Abdulhusein Mohsin Al-Sudani, & Iskender Akkurt. (2025). The Experimental Enhancing of the Radiation Shield Properties of Some Produced Compounds. *International Journal of Applied Sciences and Radiation Research* , 2(1). https://doi.org/10.22399/ijasrar.1

[23]sengul, aycan, Toksoy, T., Kandemir, R., & Karaali, K. (2024). Feasibility of board tilt angle on critical organs during hippocampus-sparing whole-brain radiotherapy. *International Journal of Computational and Experimental Science and Engineering*, 10(1). https://doi.org/10.22399/ijcesen.292

[24] Wang Y, Qian B, Li B, et al. (2013). Metal artifacts reduction using monochromatic images from spectral CT: evaluation of pedicle screws in patients with scoliosis. *European journal of radiology*. 82(8);e360-6. doi:10.1016/j.ejrad.2013.02.024

[25] Yu L, Leng S, McCollough CH. (2012) Dual-energy CT-based monochromatic imaging. *AJR American journal of roentgenology*. 199(5 Suppl);S9-s15. doi:10.2214/ajr.12.9121

[26] Sato E, Shigemitsu R, Mito T, Yoda N, Rasmussen J, Sasaki K. (2021). The effects of bone remodeling on biomechanical behavior in a patient with an implant-supported overdenture. *Computers in biology and medicine*. 129;104173. doi:10.1016/j.compbiomed.2020.104173